JACS
JOURNAL OF THE AMERICAN CHEMICAL SOCIETY
Communication
pubs.acs.org/JACS

Spectral Tuning in Halorhodopsin: The Chloride Pump Photoreceptor

Rhitankar Pal, Sivakumar Sekharan,* and Victor S. Batista*

Department of Chemistry, Yale University, P.O. Box 208107, New Haven, Connecticut 06520-8107, United States

Supporting Information

ABSTRACT: The spectral tuning of halorhodopsin from *Halobacterium salinarum* (*sh*R) during anion transport was analyzed at the molecular level using DFT-QM/MM [SORCI+Q//B3LYP/6-31G(d):Amber96] hybrid methods. Insights into the influence of Cl^- depletion, Cl^- substitution by N_3^- or NO_3^-, and mutation of key amino acid residues along the ion translocation pathway (H95A, H95R, Q105E, R108H, R108I, R108K, R108Q, T111V, R200A, R200H, R200K, R200Q, and T203V) were analyzed for the first time in a fully atomistic model of the *sh*R photoreceptor. We found evidence that structural rearrangements mediated by specific hydrogen bonds of internal water molecules and counterions (D238 and Cl^-) in the active site induce changes in the bond-length alternation of the all-*trans* retinyl chromophore and affect the wavelength of maximal absorption in *sh*R.

Halorhodopsin from the archaeon *Halobacterium salinarum* (*sh*R) is a transmembrane retinal protein that pumps Cl^- ions into the cell upon yellow-light absorption (λ = 500−650 nm, $\lambda_{max} \approx$ 580 nm), sustaining a concentration gradient against the membrane potential (90−150 mV).[1] While *sh*R has been extensively investigated by biochemical studies[2] and structurally resolved by X-ray crystallography,[3] structure−function relationships associated with spectral tuning and ion translocation remain to be understood at the molecular level. Understanding the Cl^- pumping mechanism triggered by photoabsorption is essential for a variety of technological developments ranging from bioinspired materials for solar energy conversion[4] to studies of optogenetics[5,6] (i.e., the use of light to control the activity of genetically modified cells such as neurons that express halorhodopsin and can be silenced or desynchronized with yellow light).[7,8] In this work, we focused on spectral tuning in *sh*R as influenced by Cl^- depletion or substitution by other anions and by mutation of key amino acid residues along the ion translocation channel.

Like other retinal proteins, *sh*R folds into a barrel of seven transmembrane α-helices (named A−G) interconnected by short loops (Figure 1 left). The retinyl chromophore is covalently bound to K242 in helix G via a protonated Schiff base (pSB), dividing the Cl^- channel into two segments including the cytoplasmic (CP) and extracellular (EC) parts. Upon light absorption ($\lambda_{max} \approx$ 580 nm), the chromophore undergoes all-*trans*/13-*cis* isomerization on the picosecond time scale, causing a shift in its absorption to 600 nm (Figure 1 right, first step).[9] The isomerization is followed by Cl^- displacement in the EC side of the channel (near T111/R108, next to the pSB) on the microsecond time scale, which shifts the photoabsorption

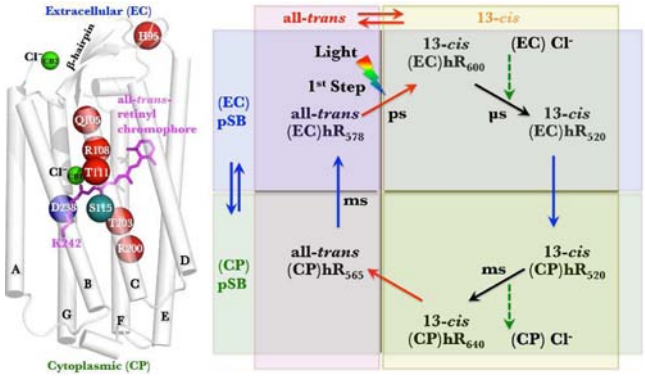

Figure 1. (left) DFT-QM/MM model of *sh*R showing the Cl^- pathway (dotted arrows), which is divided into the extracellular (EC) and cytoplasmic (CP) segments by the retinyl chromophore in the middle (magenta). Color key: H95, Q105, R108, T111, R200, T203, D238 (red spheres); Cl^- at CB1 and CB2 (green spheres); S115 (cyan sphere). (right) Cl^- pumping cycle based on all-*trans*/13-*cis* isomerization (red arrows) and EC/CP switching of the pSB (blue arrows).

to 520 nm. The pSB then switches its accessibility from the EC side to the CP side, a rearrangement that induces directionality of Cl^- transport into the cell. The displaced Cl^- then moves to the CP side on the millisecond time scale, probably through T203/R200, and the chromophore λ_{max} shifts to 640 nm. Subsequent thermal isomerization back to the all-*trans* form shifts the absorption to 565 nm. The accessibility of the pSB to the EC side is re-established on the millisecond time scale, shifting the absorption back to 580 nm for the next cycle. Remarkably, the SB remains protonated throughout the whole cycle, ensuring both thermal isomerization and photoabsorption near the maximum of the solar spectrum.

*sh*R has been relatively unexplored in comparison with its closest counterpart, bacteriorhodopsin (bR), the proton-pump photoreceptor from *H. salinarum*.[10] However, both *sh*R and bR are ion pumps driven by photoinduced isomerization of the retinyl chromophore.[11] Structural differences lead to differences in function, such as the proton-acceptor and proton-donor sites D85 and D96 in bR that correspond to the neutral residues T111 and A122, respectively, in *sh*R. Other structural differences include sites involved in proton release in bR (e.g., R82, E194, E204, and internal water molecules).[12] In particular, E204 corresponds to T230 in *sh*R.[12] These differences are critical for functionality,[12] as confirmed by the conversion of bR into a Cl^- pump upon D85T mutation.[13,14] Analogously, mutations of *sh*R affect the Cl^- transport.[15,16]

Received: May 8, 2013
Published: June 18, 2013

   dx.doi.org/10.1021/ja404600z | J. Am. Chem. Soc. 2013, 135, 9624−9627

Site-directed mutagenesis studies of *sh*R have probed several of the amino acid residues involved in the ion translocation pathway (Figure 1 left).[15,16] For example, H95 (conserved in all classes of hR and situated in EC loop B−C) is critical for ion pumping, as H95A and H95R mutations decrease the pumping rate 20-fold relative to the wild type (WT).[15] Furthermore, mutations of sites Q105, R108, and T111 (Q105E, R108H, R108I, R108K, R108Q, and T111V) reduce the Cl^- transport by 25%,[16] while mutations of R200 (R200A, R200H, R200K, and R200Q) and T203 (T203V) in helix F toward the CP side reduce the Cl^- transport quite drastically.[15] However, the underlying structural rearrangements induced by these point-site mutations remain poorly understood. In this work, we analyzed the effect of mutations on specific interactions using density functional theory (DFT) and hybrid quantum mechanics/molecular mechanics (QM/MM) methods.[17,18]

We compared WT *sh*R and single-point mutants for which experimental mutagenesis data are available.[15,16] The DFT-QM/MM models were based on the 1.8 Å resolution X-ray structure of *sh*R (PDB entry 1E12)[7] and were prepared according to the ONIOM scheme with electronic embedding (EE)[18] as implemented in Gaussian 09[19] [for further details, see section I in the Supporting Information (SI)]. The analysis of spectral tuning involved calculations of $S_1 \leftarrow S_0$ vertical excitations at the SORCI+Q//B3LYP/6-31G(d): Amber96 level of theory.[20−22] This methodology typically yields results in good agreement with experiments (within ±20 nm), as shown for other retinal proteins.[23,24] We analyzed the influence exerted by counterions in models prepared with protonated (neutral) D238 and/or with Cl^- replaced by N_3^- or NO_3^-. In addition, we analyzed the effects produced by displacement of internal water molecules and reorganization of H-bonds in the active site. Finally, we analyzed the S115D and S115E mutations without Cl^- to mimic the counterion (D85) of bR.

The DFT-QM/MM analysis showed that the photoabsorption λ_{max} of the retinyl chromophore is sensitive to the strength of the interaction between the pSB and the counterion (Cl^- or D238 upon Cl^- displacement; Figure 2). In particular, the absorption of the WT at ∼580 nm requires Cl^- (or another anion such as N_3^- or NO_3^-) to be in the proximity of the chromophore, while Cl^- depletion (or protonation of D238) induces a red shift in the absorption to 620−630 nm (Figure 2). As for other retinal proteins,[23,24] λ_{max} is linearly correlated with the attenuation of the bond-length alternation (BLA, defined as the average bond length of single bonds in the C5−N_{SB}^+ segment minus the average bond length of double bonds in that segment). *sh*R models with counterions have a typical BLA of ∼0.04 Å, while the BLA of ∼0.02 Å in models without Cl^- (or with protonated D238) is significantly lower (Figure 2 inset).

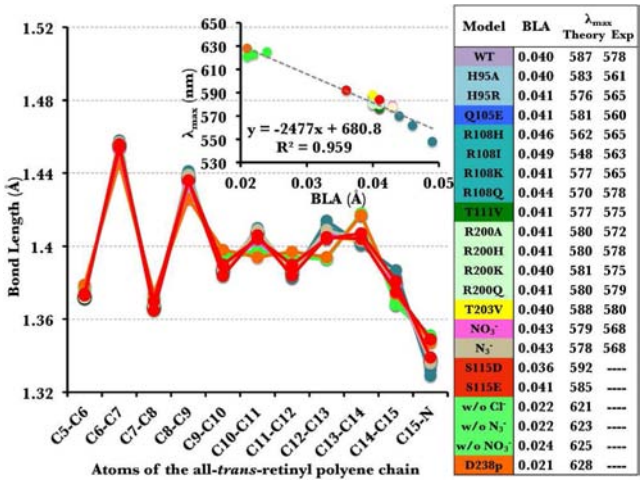

Model	BLA	λ_{max} Theory	Exp
WT	0.040	587	578
H95A	0.040	583	561
H95R	0.041	576	565
Q105E	0.041	581	560
R108H	0.046	562	565
R108I	0.049	548	563
R108K	0.041	577	565
R108Q	0.044	570	578
T111V	0.041	577	575
R200A	0.041	580	572
R200H	0.041	580	578
R200K	0.040	581	575
R200Q	0.041	580	579
T203V	0.040	588	580
NO_3^-	0.043	579	568
N_3^-	0.043	578	568
S115D	0.036	592	----
S115E	0.041	585	----
w/o Cl^-	0.022	621	----
w/o N_3^-	0.022	623	----
w/o NO_3^-	0.024	625	----
D238p	0.021	628	----

Figure 2. Bond lengths along the all-*trans* retinyl chromophore in DFT-QM/MM structural models of WT *sh*R and *sh*R mutants. The inset shows the correlation between the BLA and the calculated value of λ_{max}.

The observed differences in λ_{max} among the various mutants (Figure 2) can be traced back to electrostatic effects and to the difference in the total number of intermolecular H-bonding networks in the active site that induce changes in the chromophore BLA (see section IX in the SI).[25] In fact, an increase in BLA is usually correlated with a decrease in λ_{max}. For example, the S115D and S115E mutants decrease the BLA, inducing a red shift in λ_{max} relative to the WT. These results suggest that in the absence of Cl^-, the carboxylate groups introduced by the S115D and S115E single-point mutations can mimic the functionality of counterions to the pSB. In contrast, substitution of Cl^- by NO_3^- or N_3^- changes the BLA only slightly (from 0.040 to 0.043 Å), inducing a small blue shift in λ_{max} from 587 to ∼578 nm.

Water molecules bound in the active site are essential for protein functionality.[26] In our DFT-QM/MM models of *sh*R, three water molecules (w2023, w2081, and w2082) were found to be directly H-bonded to Cl^-. Two of them (w2081 and w2082) are also H-bonded to D238, while the third one (w2023) shares a H-bond with the OH group of S76. The resulting structure of the H-bonds is similar to the H-bonding network in the active site of bR, where three water molecules (w401, w402, and w406) and two counterions (D212 and D85) correspond to the three water molecules (w2081, w2082, and w2023) and the two counterions (D238 and Cl^-) in *sh*R (Figure 3). The main

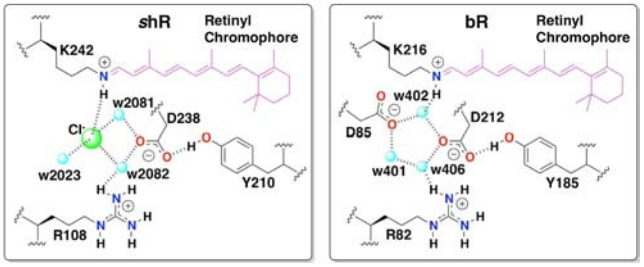

Figure 3. Comparison of (left) the diamond-shaped water cluster in *sh*R and (right) the pentagonal water cluster in bR mediated by H-bonds in the active site.

difference between the two networks involves the H-bonding of the counterions with the pSB. In *sh*R, Cl^- interacts directly with the pSB, while the D85 counterion in bR is more restrained and therefore interacts with the pSB only indirectly through w402. As a result, the three waters and counterions in bR form a pentagonal network of H-bonds,[27−29] whereas in *sh*R a diamond-shaped ring of H-bonds is formed as a result of displacement of w2023 toward S76 (Figure 3). These bound waters form key H-bonds that regulate the interaction of the pSB with the counterions.[29]

Site H95: The amino acid residue H95 is located at the center of the B−C loop and is H-bonded to P92, L97, and w2020, ∼24 Å away from chloride binding site 1 (CB1) (Figure 1 left). The B−C loop has a β-hairpin secondary structure stabilized by three H-bonds to backbone atoms of residues I89, V102, M91, and

dx.doi.org/10.1021/ja404600z | J. Am. Chem. Soc. 2013, 135, 9624−9627

E100, ~20 Å away from chloride binding site 2 (CB2). These interactions are affected in the H95R mutant, in which there are two more H-bonds involving G87 and S104. These additional H-bonds perturb the R103−Cl^- interaction, which in turn affects the binding of Cl^- at CB2 (see section IV in the SI). Experimental studies of the H95R and H95A mutants suggested that the pumping activity is reduced at low Cl^- concentration but not under physiological conditions.[15] These observations are consistent with minor perturbations that might affect the B−C loop and the CB2 site but do not fully prevent Cl^- transport.

Site Q105: The amino acid residue Q105 is H-bonded to R108, >10 Å away from the active site and quite far from both CB1 and CB2. Remarkably, mutation of Q105 to glutamate (Q105E) suppresses the Cl^- transport by ~25% and induces a blue shift in λ_{max}. However, the structural rearrangements are predicted to be only modest because residue 105 remains H-bonded to R108, with the carboxylate group of E105 functioning as a H-bond acceptor (see section V in the SI). Therefore, we suggest that the glutamate side chain must establish an electrostatic barrier for Cl^- translocation.

Site R108: The conserved amino acid residue R108 (in helix C) corresponds to R82 in bR and R123 in hR from *Natronobacterium pharaonis* (*p*hR) (see section II in the SI). As shown in Figure 4, the DFT-QM/MM models predict that the side chain

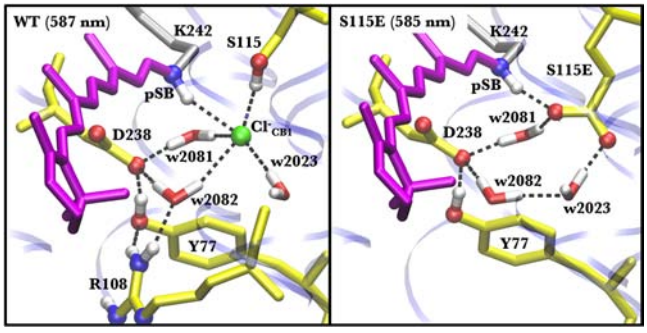

Figure 4. H-bonding networks in the active sites of (left) WT *s*hR and (right) the S115E mutant.

of R108 is H-bonded to Y77 and w2082 (the bound water molecule H-bonded to D238 and Cl^- at CB1). The mutations R108H, R108I, and R108K lead to the loss of the H-bond with w2082, while this important H-bond is preserved in R108Q. These perturbations of H-bonds correlate with the experimental observation that the R108H, R108I, and R108K mutants exhibit reduced Cl^- transport activity relative to R108Q,[16b] the expected trend for mutants with more structural disorder along the Cl^- channel induced by a decrease in the number of H-bonds.

Site T111: The amino acid residue T111 is very close to CB1 (Figure 1), with the Cl^- almost equidistant from the OH of T111 (5.91 Å) and the NH_2 of R108 (5.17 Å). The OH group of T111 is H-bonded to the backbone carbonyl of G107, which is situated only one helical turn away. This H-bond is broken upon T111V mutation (see section V in the SI), producing a structural rearrangement that might be responsible for the observed 25% reduction in the pumping rate.[16]

Sites R200 and T203: R200 and T203 (in helix F) are ~14 and ~9 Å away from the pSB, so the side chains of these residues are too far away from the active site to interact directly with the pSB. However, the T203V mutation has been shown to reduce the Cl^- transport activity. The DFT-QM/MM model showed that substitution of T with V breaks the H-bond between the OH group of T203 and the backbone carbonyl of L199 (similar to the rearrangements in the T111V mutant). However, the H-bond between the NH group of T203 and the backbone carbonyl of L199 remains intact during the T203V mutation (see section V in the SI). Therefore, it is evident that loss of the H-bond with L199 and the proximity of site 203 to CB1 must account for the observed reduction in Cl^- transport upon mutation. Compared with R108 mutants, R200 mutants have not been found to have a drastic effect on the Cl^- pumping activity,[16] probably because R200 is situated far away from CB1.

Other anions: *s*hR can transport several other anions into the cell besides Cl^-. Therefore, we modeled NO_3^- and N_3^- ions in the active site (Figure 5), since like Cl^- they can impart a negative

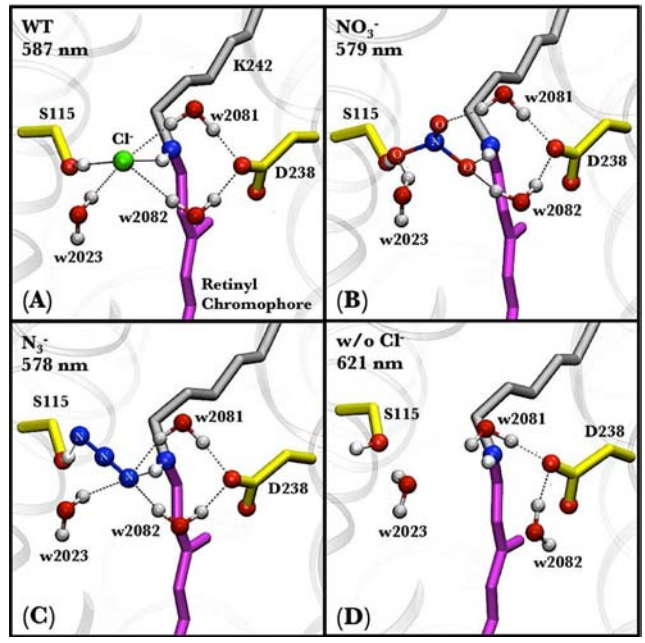

Figure 5. Comparison of the binding site models (A) with Cl^-, (B) with NO_3^-, (C) with N_3^-, and (D) without Cl^-.

charge. Moreover, NO_3^- and N_3^- differ in shape and size, allowing an analysis of both electrostatic and steric factors that might affect the active site of *s*hR. Substitution of Cl^- with NO_3^- or N_3^- does not significantly affect the nature of the H-bonding with D238 or the two bound water molecules at the active site (w2081 and w2082) (Figure 5). In binding of N_3^-, the terminal nitrogen (N1) forms a H-bond with S115 while the central nitrogen atom (N2) interacts with w2023 and w2081. In the case of NO_3^-, two of the three O atoms form H-bonds with the SB, w2082, w2023, and S115, while w2081 donates H-bonds to the third O atom and D238. Even when the ions differ in size and shape (Cl^-, NO_3^-, and N_3^-), the architecture of the H-bonding network in the active site remains conserved.

Site S115: The amino acid residue S115 is unique since it is the only one that can establish a direct H-bond with Cl^- at CB1. Substitution of S115 with D or E places a carboxylate group ~2.70 Å from the pSB (Figure 4 right). The negative charge of this carboxylate can mimic the electrostatic effect of Cl^- and produce a comparable spectral shift (Figure 2). Furthermore, the presence of D or E at site 115 is similar to the presence of D at site 85 in bR. The main difference is that S115D/E forms a *direct* H-bond with the pSB (Figure 4), whereas D85 in bR forms an *indirect* H-bond with the pSB mediated by w402 (Figure 3). This

dx.doi.org/10.1021/ja404600z | *J. Am. Chem. Soc.* 2013, 135, 9624−9627

structural difference might explain the unsuccessful attempts to convert *p*hR (a Cl^- pump) into bR (a proton pump)[30] by mutation at site S130 (analogous to S115 in *s*hR).

In summary, our DFT-QM/MM structural analysis of WT *s*hR and single-point mutations of key amino acid residues provides fundamental insights into the molecular origin of spectral tuning and ion stability along the translocation pathway, as determined by specific H-bonding interactions or ion-displacement/substitution. While many of the resulting changes are subtle, it is clear that the underlying rearrangements of H-bonds induce structural changes that affect ion intake from the extracellular side, ion displacement through the translocation channel, and electrostatic interactions between the pSB and its surroundings at the active site. These molecular-level insights correlate with key experimental observations and also provide several testable predictions that can aid in the selection of new ion-pump photoreceptors for optogenetics.

■ ASSOCIATED CONTENT

Supporting Information

Primary sequence alignment, system setup, geometrical parameters of the retinyl chromophore, key hydrogen bonding distances, and complete ref 19. This material is available free of charge via the Internet at http://pubs.acs.org.

■ AUTHOR INFORMATION

Corresponding Author

sivakumar.sekharan@yale.edu; victor.batista@yale.edu

Notes

The authors declare no competing financial interest.

■ ACKNOWLEDGMENTS

The authors thank Jennifer N. Wei for assistance with the sequence alignment and acknowledge supercomputer time from the National Energy Research Scientific Computing Center (NERSC) and support from the National Science Foundation (CHE-0911520).

■ REFERENCES

(1) (a) Lanyi, J. K.; Oesterhelt, D. *J. Biol. Chem.* **1982**, *257*, 2674. (b) Mehlhorn, R. J.; Schobert, B.; Packer, L. *Biochim. Biophys. Acta* **1985**, *809*, 66.

(2) (a) Lanyi, J. K. *Physiol. Rev.* **1990**, *70*, 319. (b) Birge, R. R. *Biochim. Biophys. Acta* **1990**, *1016*, 293. (c) Birge, R. R.; Cooper, T. M.; Lawrence, A. F.; Masthay, M. B.; Zhang, C.-F.; Zidovetzki, R. *J. Am. Chem. Soc.* **1991**, *113*, 4327. (d) Bamberg, E.; Tittor, J.; Oesterhelt, D. *Proc. Natl. Acad. Sci. U.S.A.* **1993**, *90*, 639. (e) Oesterhelt, D. *Isr. J. Chem.* **1995**, *35*, 475. (f) Haupts, U.; Tittor, J.; Bamberg, E.; Oesterhelt, D. *Biochemistry* **1997**, *36*, 2. (g) Oesterhelt, D. *Curr. Opin. Struct. Biol.* **1998**, *8*, 489. (h) Lanyi, J. K. *J. Phys. Chem. B* **2000**, *104*, 11441.

(3) Kolbe, M.; Besir, H.; Essen, L.-O.; Oesterhelt, D. *Science* **2000**, *288*, 1390.

(4) Xu, J.; Vanderlick, T. K.; LaVan, D. A. *Int. J. Photoenergy* **2012**, No. 425735.

(5) Zhang, F.; Wang, L.-P.; Brauner, M.; Liewald, J. F.; Kay, K.; Watzke, N.; Wood, P. G.; Bamberg, E.; Nagel, G.; Gottschalk, A.; Deisseroth, K. *Nature* **2007**, *446*, 633.

(6) Chow, B.; Han, X.; Dobry, A. S.; Qian, X.; Chuong, A. S.; Li, M.; Henninger, M. A.; Belfort, G.; Lin, Y.; Monahan, P. E.; Boyden, E. S. *Nature* **2010**, *463*, 98.

(7) Deisseroth, K. *Nat. Methods* **2011**, *8*, 26.

(8) Hegemann, P.; Möglich, A. *Nat. Methods* **2011**, *8*, 39.

(9) Varo, G.; Zimányi, L.; Fan, X.; Sun, L.; Needleman, R.; Lanyi, J. K. *Biophys. J.* **1995**, *68*, 2062.

(10) (a) Ren, L.; Martin, C. H.; Wise, K. J.; Gillespie, N. B.; Luecke, H.; Lanyi, J. K.; Spudich, J. L.; Birge, R. R. *Biochemistry* **2001**, *40*, 13906. (b) Hayashi, S.; Tajkhorshid, E.; Pebay-Peyroula, E.; Royant, A.; Landau, E. M.; Navarro, J.; Schulten, K. *J. Phys. Chem. B* **2001**, *105*, 10124. (c) Sakurai, M.; Sakata, K.; Saito, S.; Nakajima, S.; Inoue, Y. *J. Am. Chem. Soc.* **2003**, *125*, 3108. (d) Kloppmann, E.; Becker, T.; Ulmann, G. M. *Proteins* **2005**, *61*, 953.

(11) Lanyi, J. K. *Annu. Rev. Biophys. Chem.* **1986**, *15*, 11.

(12) Varo, G. *Biochim. Biophys. Acta* **2000**, *1460*, 220.

(13) Sasaki, J.; Brown, L. S.; Chon, Y. S.; Kandori, H.; Maeda, A.; Needleman, R.; Lanyi, J. K. *Science* **1995**, *269*, 73.

(14) Tittor, J.; Haupts, U.; Haupts, C.; Oesterhelt, D.; Becker, A.; Bamberg, E. *J. Mol. Biol.* **1997**, *271*, 405.

(15) Otomo, J. *Biochemistry* **1996**, *35*, 6684.

(16) (a) Rüdiger, M.; Haupts, U.; Gerwert, K.; Oesterhelt, D. *EMBO J.* **1995**, *14*, 1599. (b) Rüdiger, M.; Oesterhelt, D. *EMBO J.* **1997**, *16*, 3813. (c) Paula, S.; Tittor, J.; Oesterhelt, D. *Biophys. J.* **2001**, *80*, 2386.

(17) Warshel, A.; Levitt, M. *J. Mol. Biol.* **1976**, *103*, 227.

(18) Vreven, T.; Morokuma, K.; Farkas, O.; Schlegel, H. B.; Frisch, M. J. *J. Comput. Chem.* **2003**, *24*, 760.

(19) Frisch, M. J.; et al. *Gaussian 09*, revision A.02; Gaussian, Inc.: Wallingford, CT, 2009.

(20) Neese, F. A. *J. Chem. Phys.* **2003**, *119*, 9428.

(21) Neese, F. *ORCA: An ab Initio DFT and Semiempirical Electronic Structure Package*, version *2.6*; 2007.

(22) Cornell, W. D.; Cieplak, P.; Bayly, C. I.; Gould, I. R.; Merz, K. M.; Ferguson, D. M.; Spellmeyer, D. C.; Fox, T.; Caldwell, J. W.; Kollman, P. A. *J. Am. Chem. Soc.* **1995**, *117*, 5179.

(23) (a) Sekharan, S.; Altun, A.; Morokuma, K. *Chem.—Eur. J.* **2010**, *16*, 1744. (b) Sekharan, S.; Morokuma, K. *J. Phys. Chem. Lett.* **2010**, *1*, 668. (c) Sekharan, S.; Altun, A.; Morokuma, K. *J. Am. Chem. Soc.* **2010**, *132*, 15856. (d) Sekharan, S.; Morokuma, K. *J. Am. Chem. Soc.* **2011**, *133*, 4734. (e) Sekharan, S.; Morokuma, K. *J. Am. Chem. Soc.* **2011**, *133*, 19052. (f) Sekharan, S.; Yokoyama, S.; Morokuma, K. *J. Phys. Chem. B* **2011**, *115*, 15380. (g) Sekharan, S.; Altun, A.; Morokuma, K. *Annu. Rep. Comput. Chem.* **2011**, *7*, 215. (h) Sekharan, S.; Katayama, K.; Kandori, H.; Morokuma, K. *J. Am. Chem. Soc.* **2012**, *134*, 10706.

(24) (a) Gascon, J. A.; Batista, V. S. *Biophys. J.* **2004**, *87*, 2931. (b) Gascon, J. A.; Sproviero, E. M.; Batista, V. S. *J. Chem. Theory Comput.* **2005**, *1*, 674. (c) Gascon, J. A.; Sproviero, E. M.; Batista, V. S. *Acc. Chem. Res.* **2006**, *39*, 184. (d) Sekharan, S.; Wei, J. N.; Batista, V. S. *J. Am. Chem. Soc.* **2012**, *134*, 19536.

(25) (a) Zhao, G. J.; Liu, J. Y.; Zhou, L. C.; Han, K. L. *J. Phys. Chem. B* **2007**, *111*, 8940. (b) Zhao, G. J.; Han, K. L. *Biophys. J.* **2008**, *94*, 38. (c) Zhao, G. J.; Han, K. L. *Acc. Chem. Res.* **2012**, *45*, 404.

(26) Angel, A. E.; Chance, M. R.; Palczewski, K. *Proc. Natl. Acad. Sci. U.S.A.* **2009**, *106*, 8555.

(27) Kandori, H.; Yoshihara, K.; Tomioka, H.; Sasabe, H. *J. Phys. Chem.* **1992**, *96*, 6066.

(28) Shibata, M.; Kandori, H. *Biochemistry* **2005**, *44*, 7406.

(29) Luecke, H.; Schobert, B.; Richter, H.-T.; Cartailler, J.-P.; Lanyi, J. K. *J. Mol. Biol.* **1999**, *291*, 899.

(30) Muroda, K.; Nakashima, K.; Shibata, M.; Demura, M.; Kandori, H. *Biochemistry* **2012**, *51*, 4677.